materials

MDPI

Article

Thermoanalytical and X-ray Diffraction Studies on the Phase Transition of the Calcium-Substituted $La_2Mo_2O_9$ System

Artūras Žalga * and Giedrė Gaidamavičienė

Department of Applied Chemistry, Faculty of Chemistry and Geosciences, Vilnius University, Naugarduko Str. 24, 03225 Vilnius, Lithuania
* Correspondence: arturas.zalga@chf.vu.lt

Abstract: An aqueous sol-gel preparation technique was applied for the synthesis of calcium-substituted lanthanum molybdate with the initial composition of $La_{2-x}Ca_xMo_2O_{9-x/2}$. The influence of the substitution effect, which plays a crucial role in the formation of final ceramics, was investigated. The thermal behavior tendencies of phase transition at elevated temperatures from the monoclinic crystal phase to cubic as well as reversible transformation were identified and discussed in detail. It was proved that the phase transformation in the obtained mixture significantly depends only on the impurities' amount, while the partial substitution by calcium atoms above the value of x = 0.05 does not create a homogeneous multicomponent system for $La_{2-x}Ca_xMo_2O_{9-x/2}$ composition.

Keywords: sol-gel synthesis; phase transition; thermal analysis; X-ray diffraction; Rietveld refinement

Citation: Žalga, A.; Gaidamavičienė, G. Thermoanalytical and X-ray Diffraction Studies on the Phase Transition of the Calcium-Substituted $La_2Mo_2O_9$ System. *Materials* **2023**, *16*, 813. https://doi.org/10.3390/ma16020813

Academic Editor: Joan-Josep Suñol

Received: 9 December 2022
Revised: 6 January 2023
Accepted: 11 January 2023
Published: 13 January 2023

1. Introduction

Since the discovery of enhanced ionic conductivity for the $La_2Mo_2O_9$ compound by Lacorre in 2000 [1], the efforts of application [2] for this system in different electrochemical devices have continuously increased [3]. Oxygen pumps, sensors, and solid oxide fuel cells (SOFCs) [4–7] are only a few types of equipment where lanthanum molybdenum oxide can be successfully applied. Despite a reversible phase transformation [8,9] above 540 °C from a low-temperature form α-$La_2Mo_2O_9$ [10] to a high-temperature form β-$La_2Mo_2O_9$ [11], its chemical stability [12] under air atmosphere in the range of temperature from 600 °C to 1000 °C creates the conditions for using this compound as a solid electrolyte of oxygen ions [13]. Moreover, the densification [14] of the corresponding ceramic could be successfully applied below the temperature of 1200 °C while creating desirable surface and crystalline properties [15,16]. The synthesis technique [17–19] that allows the preparation of the initial mixture of lanthanum and molybdenum oxides also plays an important role during the formation of the final ceramic at high temperatures. However, the molar ratio of initial metals remains the main factor that determines the formation of the $La_2Mo_2O_9$ composition. This is the reason why the partial substitution [20–22] of either lanthanum [23–25] or molybdenum [26–29] leads to the crystallization of side phases [30,31], which significantly affects the physical properties [32,33] of the corresponding compound. This effect is directly related to both the amount of the $La_2Mo_2O_9$ phase in the final ceramic mixture and the increased stabilization of the cubic phase at room temperature. Therefore, the main aim of this work was to study the dependence of the phase transition of $La_2Mo_2O_9$ ceramics on the degree of calcium substitution in the corresponding system.

2. Materials and Methods

La–Ca–Mo–O tartrate gel precursor for $La_{2-x}Ca_xMo_2O_{9-x/2}$ ceramic was prepared by an aqueous sol-gel synthesis using tartaric acid as a chelating agent that interacts as a ligand at the molecular level with the reaction mixture during both the dissolution in water and either sol or gel formation. The general scheme of this experiment is illustrated and presented in Figure 1.

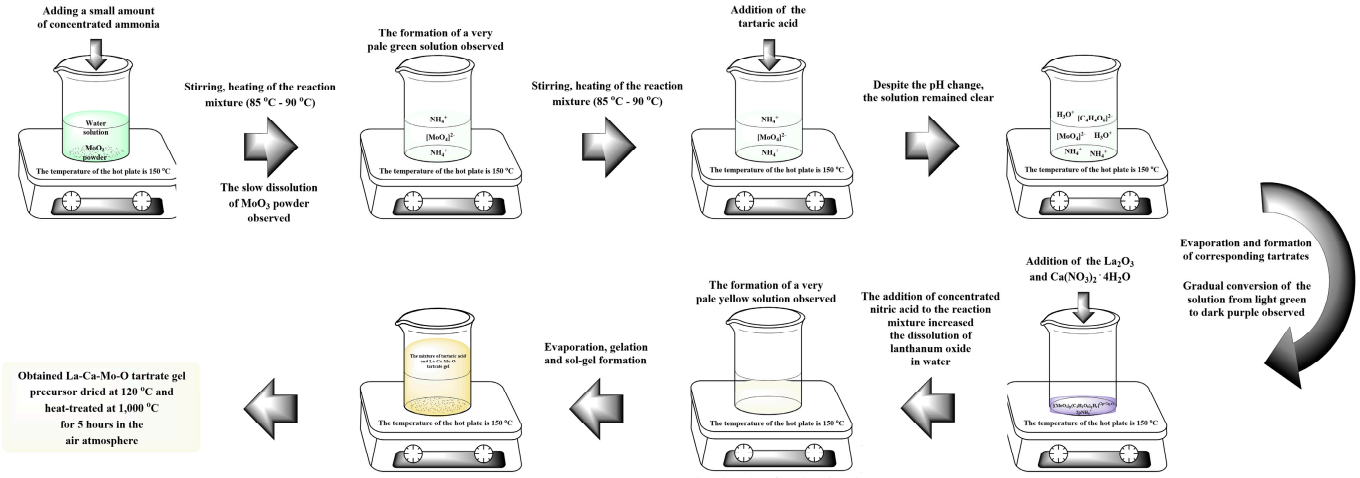

Figure 1. Synthesis scheme of the La–Ca–Mo–O tartrate precursor for $La_{2-x}Ca_xMo_2O_{9-x/2}$ ceramic.

Lanthanum (III) oxide (La_2O_3, 99.99% Alfa Aesar), molybdenum (VI) oxide (MoO_3, 99.95% Alfa Aesar), and calcium (II) nitrate tetrahydrate ($Ca(NO_3)_2 \cdot 4H_2O$ 99.98% Alfa Aesar) were used as starting materials and weighed before the dissolution procedure according to the desired stoichiometric ratio. It should be noted that, despite the high purity of the lanthanum (III) oxide, it was additionally heat-treated at 1000 °C for 5 h because of its tendency of the reaction with humidity and carbon dioxide from the air. In this case, even a slight deviation in the lanthanum amount from the ideal composition for $La_2Mo_2O_9$ ceramic creates conditions for the formation of impurity phases such as $La_2Mo_3O_{12}$ or La_2MoO_6 [34]. Nitric acid (HNO_3 66% Reachem (Mississauga, Canada)), distilled water, and concentrated ammonia solution ($NH_3 \cdot H_2O$ 25% Penta (Prague, Czech Republic)) were used as solvents and reagents to regulate the pH of the solution. Tartaric acid (L–(+)–Tartaric acid ($C_4H_6O_6$) (TA) $\geq$ 99.5% Sigma-Aldrich (Darmstadt, Germany)) was applied for escalation of solubility via coordination of starting compounds in the reaction mixture, especially during the pH changes and evaporation before sol-gel formation. The mechanism of the corresponding chemical process in the frame of the aqueous tartaric acid-assisted synthesis for the preparation of the La–Mo–O gel precursor was discussed in our previous work [35]. Finally, the obtained La−Ca−Mo−O tartrate gel precursor for $La_{2-x}Ca_xMo_2O_{9-x/2}$ ceramics was heat-treated for 5 h at 1000 °C in the air atmosphere.

The thermal analysis of heat-treated powders was performed with TG–DSC, with a STA 6000 PerkinElmer instrument using a sample mass of about 20 mg and a heating rate of 40 °C min^{-1} under an airstream of 20 $cm^3 \cdot min^{-1}$ at ambient pressure. The heating and cooling cycle was fulfilled twice from 300 °C to 800 °C and from 800 °C to 300 °C. The sample mass, heating rate, atmosphere, and its flow rate were selected empirically during numerous tests to ensure the best signal peak efficiency and to minimize the noises and background signals, which occur because of the influence of the corundum crucible and equipment limits. The characteristics of the phase transition peak were evaluated in the ranges of temperature from 530 °C to 600 °C for heating and from 560 °C to 490 °C for the cooling regime. X-ray diffraction (XRD) patterns were recorded in air at room temperature by employing a powder X-ray diffractometer Rigaku MiniFlex II using CuKα_1 radiation. XRD patterns were recorded at the standard rate of 1.5 2θ min^{-1}. The sample was spread on the glass holder to obtain the maximum intensity of the characteristic peaks in the XRD diffractograms. The Rietveld refinements of the obtained XRD patterns were performed using X'Pert HighScore Plus version 2.0a software.

3. Results and Discussion

3.1. Thermal Analysis

In this work, thermal analysis as a powerful investigation technique was used for a detailed investigation of the crystal phase transition from the monoclinic α-phase to

cubic β-phase and from the cubic β-phase to monoclinic α-phase in the $La_{2-x}Ca_xMo_2O_{9-x/2}$ ceramic system. An example of a differential scanning calorimetry (DSC) curve for the $La_{1.95}Ca_{0.05}Mo_2O_{8.975}$ compound is presented in Figure 2. The corresponding results for other samples are presented in the Appendix A. Meanwhile, the data of the phase transition during the repeated heat treatments are collected in Table 1.

Table 1. Thermoanalytical data and α↔β phase transition peak properties for $La_{2-x}Ca_xMo_2O_{9-x/2}$ ceramic.

Initial Composition	Sample Mass/mg	Heating/Cooling Stages		Temperature/°C			Heat	
				Onset	End	Peak Position	Flow/mJ	Enthalpy/J·g^{-1}
$La_2Mo_2O_9$	20.181	heating	stage I	556.07	579.33	563.25	195.047	9.665
			stage II	555.69	578.84	563.03	204.953	10.1559
		cooling	stage I	540.31	523.80	533.34	–146.255	–7.2473
			stage II	540.26	523.17	533.29	–147.886	–7.3281
$La_{1.999}Ca_{0.001}Mo_2O_{8.9995}$	22.158	heating	stage I	558.63	580.56	567.11	191.073	8.6231
			stage II	556.36	578.06	564.68	209.688	9.4632
		cooling	stage I	537.43	511.92	525.65	–156.176	–7.0482
			stage II	537.45	511.92	526.09	–153.356	–6.9209
$La_{1.99}Ca_{0.01}Mo_2O_{8.995}$	22.153	heating	stage I	562.12	585.08	569.41	194.41	8.7757
			stage II	559.49	582.62	566.63	197.462	8.9134
		cooling	stage I	533.02	512.79	523.19	–145.764	–6.5798
			stage II	532.63	511.21	522.73	–142.37	–6.4266
$La_{1.95}Ca_{0.05}Mo_2O_{8.975}$	22.146	heating	stage I	565.55	587.31	573.98	183.43	8.2826
			stage II	563.28	587.47	571.59	193.262	8.7266
		cooling	stage I	527.46	497.28	517.3	–134.667	–6.0808
			stage II	527.68	498.61	518.05	–137.095	–6.1904
$La_{1.9}Ca_{0.1}Mo_2O_{8.95}$	22.183	heating	stage I	567.18	589.94	575.53	182.851	8.2429
			stage II	564.64	587.71	573.60	191.273	8.6225
		cooling	stage I	530.34	512.47	525.64	–139.347	–6.2817
			stage II	530.42	513.60	525.82	–140.215	–6.3208
$La_{1.85}Ca_{0.15}Mo_2O_{8.925}$	22.189	heating	stage I	566.04	589.64	574.53	181.146	8.146
			stage II	563.04	588.21	572.27	189.325	8.5323
		cooling	stage I	530.33	515.25	525.78	–137.468	–6.1953
			stage II	530.38	515.97	526.06	–137.764	–6.2086
$La_{1.8}Ca_{0.2}Mo_2O_{8.9}$	22.200	heating	stage I	566.1	589.06	574.45	175.753	7.9168
			stage II	563.01	585.8	571.18	183.708	8.2751
		cooling	stage I	532.05	515.17	526.57	–137.915	–6.2124
			stage II	532.12	516.21	526.66	–133.617	–6.0188
$La_{1.75}Ca_{0.25}Mo_2O_{8.875}$	22.182	heating	stage I	561.67	586.44	571.56	181.96	8.203
			stage II	547.82	573.6	556.83	182.224	8.2148
		cooling	stage I	526.46	508.12	521.81	–115.632	–5.2128
			stage II	526.48	510.01	521.98	–118.351	–5.3354
$La_{1.7}Ca_{0.3}Mo_2O_{8.85}$	22.192	heating	stage I	560.67	585.41	569.80	176.441	7.9507
			stage II	546.08	571.05	555.68	178.614	8.0486
		cooling	stage I	526.23	508.93	521.35	–111.515	–5.0250
			stage II	526.17	510.26	521.13	–113.167	–5.0995

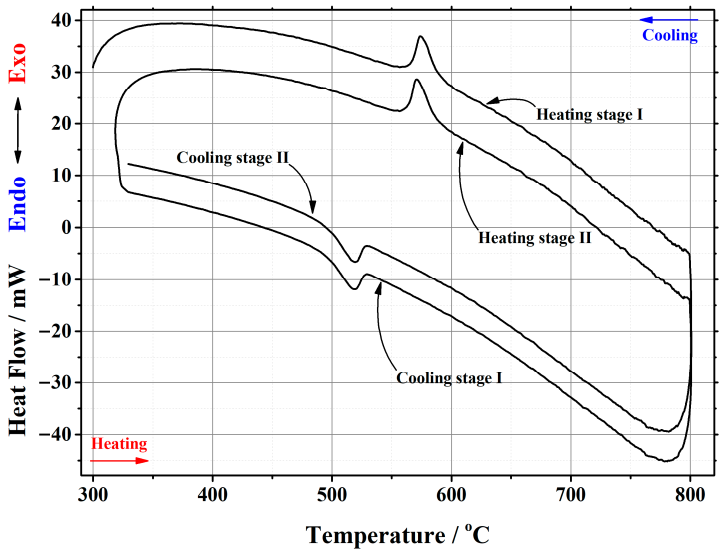

Figure 2. DSC curve of the phase transition cycles for $La_{1.95}Ca_{0.05}Mo_2O_{8.975}$ ceramic heat-treated at 1000 °C.

It is seen from Table 1 that the enthalpy values of the first heating cycle are slightly lower, especially in the cases with a smaller amount of calcium ions, compared with the second one. The reversible stabilization of the cubic phase at room temperature after partial transformation from the monoclinic α-phase determines the main reason for such behavior. According to the measurement conditions, the second heating cycle corresponds to phase transition energy more precisely. Therefore, the representation of the tendency of enthalpy change of only the second heating and cooling cycles according to the substitution degree of calcium ions is shown in Figures 3 and 4. The decrease in the tendency of phase transition enthalpy by increasing the calcium amount in the corresponding system is directly related to the amount of the monoclinic crystal phase of the $La_2Mo_2O_9$ compound. Nevertheless, during the cooling stage, the increased enthalpy of the phase transition in the $La_{1.9}Ca_{0.1}Mo_2O_{8.95}$ sample shows that the reduction of the $La_2Mo_2O_9$ phase is not the only factor that determines the energetics of the phase transition.

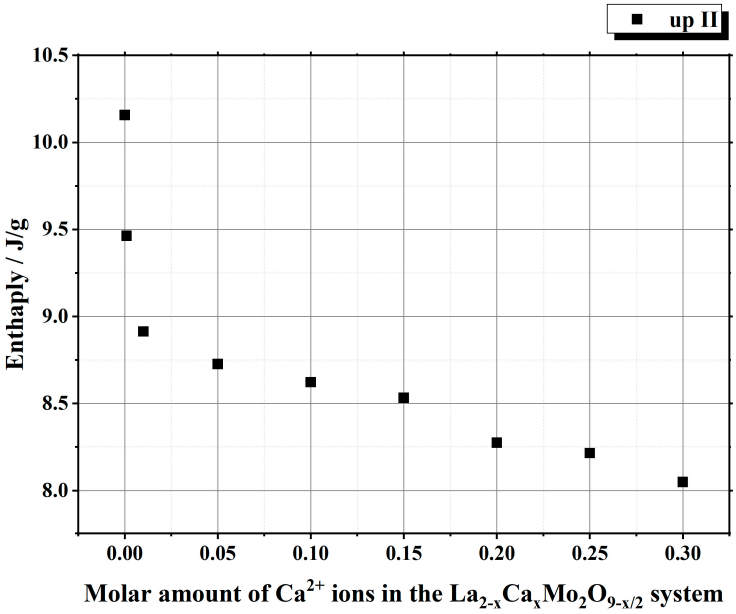

Figure 3. Dependency of the phase transition enthalpy values from the substitution degree by calcium in the $La_{2-x}Ca_xMo_2O_{9-x/2}$ system under the second heating stage.

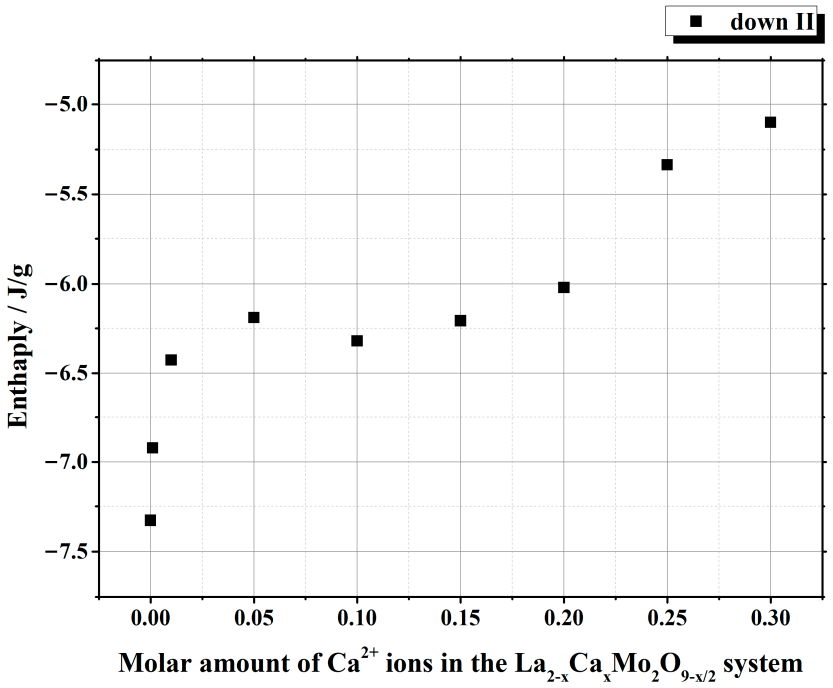

Figure 4. Dependency of the phase transition enthalpy values from the substitution degree by calcium in the $La_{2-x}Ca_xMo_2O_{9-x/2}$ system under the second cooling stage.

This phenomenon could be explained either by the increase in the amount of the monoclinic phase or by the influence of calcium ions on the formation of side phases in the final ceramic mixture. By further increasing the concentration of calcium ions in the $La_{2-x}Ca_xMo_2O_{9-x/2}$ system, the enthalpy of the phase transition starts to decrease, and this result is directly related to the decrease in the amount of the crystalline phase for $La_2Mo_2O_9$ in the final ceramic.

Summarizing the phase transition results obtained from cooling cycles, it can be concluded that homogeneous substitution by Ca^{2+} ions in the $La_{2-x}Ca_xMo_2O_{9-x/2}$ system takes place up to the value of x = 0.05. In this case, the phase transition mainly depends only on the amount of the monoclinic crystal phase in the $La_2Mo_2O_9$ ceramic homogeneously substituted by Ca^{2+} ions. The increase in enthalpy values of the phase transition for $La_{2-x}Ca_xMo_2O_{9-x/2}$ (x = 0.10 and 0.15) samples during the cooling stages could be explained by the side phase effect, which increases the amount of pure $La_2Mo_2O_9$ compound and its monoclinic phase in the final ceramic mixture.

3.2. X-ray Diffraction

In order to prove the crystalline composition in the obtained $La_{2-x}Ca_xMo_2O_{9-x/2}$ system, the XRD analysis of the corresponding ceramic was also performed. The XRD patterns of all samples that correspond to the data collected in Table 2 are presented in the Appendix B.

Table 2. Crystal system, mass fraction, crystallite size, lattice parameters, and agreement indices for the $La_{2-x}Ca_xMo_2O_{9-x/2}$ ceramic.

Initial Composition	Crystal Phase	Crystal System	Mass Fraction/%	Crystallite size/nm	Unit Cell			Weighted R Profile	Goodness of Fit
					a/pm	b/pm	c/pm		
					alpha/°	beta/°	gamma/°		
$La_2Mo_2O_9$	$La_2Mo_2O_9$	monoclinic	71.4	104.75	1431.438	2145.289	2855.431	12.99106	1.29603
					90.00000	90.42323	90.00000		
	$La_2Mo_2O_9$	cubic	28.6	47.03	715.106	715.106	715.106		
					90.00000	90.00000	90.00000		
$La_{1.999}Ca_{0.001}Mo_2O_{8.9995}$	$La_2Mo_2O_9$	monoclinic	48.9	66.33	1432.093	2145.928	2857.133	10.70047	1.87511
					90.00000	90.35913	90.00000		
	$La_2Mo_2O_9$	cubic	50.4	45.56	715.357	715.357	715.357		
					90.00000	90.00000	90.00000		
	$CaMoO_4$	tetragonal	0.7	–	–	–	–		
$La_{1.99}Ca_{0.01}Mo_2O_{8.995}$	$La_2Mo_2O_9$	monoclinic	54.1	71.50	1431.437	2145.437	2856.032	10.55389	1.79591
					90.00000	90.38470	90.00000		
	$La_2Mo_2O_9$	cubic	44.2	46.61	715.103	715.103	715.103		
					90.00000	90.00000	90.00000		
	$La_2Mo_3O_{12}$	monoclinic	1.2	41.08	1739.278	1186.510	1624.259		
					90.00000	107.93130	90.00000		
	$CaMoO_4$	tetragonal	0.5	–	–	–	–		
$La_{1.95}Ca_{0.05}Mo_2O_{8.975}$	$La_2Mo_2O_9$	monoclinic	59.1	70.52	1431.201	2145.733	2857.156	10.32976	1.76384
					90.00000	90.35389	90.00000		
	$La_2Mo_2O_9$	cubic	40.3	48.10	715.171	715.171	715.171		
					90.00000	90.00000	90.00000		
	$CaMoO_4$	tetragonal	0.6	–	–	–	–		
$La_{1.9}Ca_{0.1}Mo_2O_{8.95}$	$La_2Mo_2O_9$	monoclinic	44.5	35.83	1432.385	2140.825	2855.251	12.83825	2.41047
					90.00000	90.15601	90.00000		
	$La_2Mo_2O_9$	cubic	49.3	42.06	714.384	714.384	714.384		
					90.00000	90.00000	90.00000		
	$CaMoO_4$	tetragonal	3.8	–	–	–	–		
	$La_2Mo_3O_{12}$	monoclinic	1.4	43.47	1719.584	1166.525	1614.533		
					90.00000	108.09910	90.00000		
	La_2MoO_6	tetragonal	1.0	42.52	582.792	582.792	3031.347		
					90.00000	90.00000	90.00000		
$La_{1.85}Ca_{0.15}Mo_2O_{8.925}$	$La_2Mo_2O_9$	monoclinic	76.0	66.77	1430.812	2144.216	2854.451	16.89944	2.2630
					90.00000	90.36139	90.00000		
	$La_2Mo_2O_9$	cubic	17.1	44.52	714.631	714.631	714.631		
					90.00000	90.00000	90.00000		
	$CaMoO_4$	tetragonal	5.8	59.84	526.101	526.101	1153.607		
					90.00000	90.00000	90.00000		
	$La_2Mo_3O_{12}$	monoclinic	1.1	42.68	1732.883	1168.940	1619.405		
					90.00000	107.77000	90.00000		
$La_{1.8}Ca_{0.2}Mo_2O_{8.9}$	$La_2Mo_2O_9$	monoclinic	56.2	45.44	1428.985	2143.602	2858.397	12.46852	2.36196
					90.00000	90.31453	90.00000		
	$La_2Mo_2O_9$	cubic	36.4	46.98	714.584	714.584	714.584		
					90.00000	90.00000	90.00000		
	$CaMoO_4$	tetragonal	7.4	58.26	525.675	525.675	1151.621		
					90.00000	90.00000	90.00000		

Table 2. *Cont.*

Initial Composition	Crystal Phase	Crystal System	Mass Fraction/%	Crystallite size/nm	Unit Cell			Weighted R Profile	Goodness of Fit
					a/pm	b/pm	c/pm		
					alpha/°	beta/°	gamma/°		
$La_{1.75}Ca_{0.25}Mo_2O_{8.875}$	$La_2Mo_2O_9$	monoclinic	79.6	45.63	1430.900	2142.097	2850.290	14.09104	1.54335
					90.00000	90.29116	90.00000		
	$La_2Mo_2O_9$	cubic	12.2	39.32	714.035	714.035	714.035		
					90.00000	90.00000	90.00000		
	$CaMoO_4$	tetragonal	6.4	48.20	523.288	523.288	1146.182		
					90.00000	90.00000	90.00000		
	$La_2Mo_3O_{12}$	monoclinic	1.8	46.96	1732.404	1167.824	1617.912		
					90.00000	107.70840	90.00000		
$La_{1.7}Ca_{0.3}Mo_2O_{8.85}$	$La_2Mo_2O_9$	monoclinic	76.1	64.96	1430.166	2143.528	2854.548	13.81435	1.44730
					90.00000	90.34066	90.00000		
	$La_2Mo_2O_9$	cubic	13.8	45.66	714.447	714.447	714.447		
					90.00000	90.00000	90.00000		
	$CaMoO_4$	tetragonal	9.1	67.30	523.476	523.476	1146.807		
					90.00000	90.00000	90.00000		
	$La_2Mo_3O_{12}$	monoclinic	1.0	66.99	1733.132	1169.219	1619.159		
					90.00000	107.79630	90.00000		

Meanwhile, Figure 5 is consistent with XRD data, which show the formation process and trends of $La_{1-x}Ca_xMo_2O_{9-x/2}$ and $CaMoO_4$ crystalline phases. As it seen, the enthalpy of the phase transition for $La_2Mo_2O_9$ mostly depends on the amount of the monoclinic phase in the ceramic mixture. This assumption is confirmed by the increased stabilization of the cubic phase up to 48.0% even after insignificant substitution of lanthanum by calcium ions in the $La_{1.999}Ca_{0.001}Mo_2O_{8.9995}$ system.

Nevertheless, by a further increase in the substitution degree of lanthanum by calcium (x = 0.01 and 0.05), the amount of the monoclinic phase for the $La_2Mo_2O_9$ compound slightly increases; however, the trend of phase transition enthalpy change remains in a decreasing manner as concluded from Figure 3. Considering the fact that the amount of impurity phases in the obtained ceramics is really small, this decrease in the enthalpy of phase transition is basically determined by the increase in the concentration of the mixed-phase $La_{2-x}Ca_xMo_2O_{9-x/2}$. This statement is partially confirmed by the XRD diffractogram of the $Ca_{1.9}Ca_{0.1}Mo_2O_{8.95}$ compound, in which quite a significant amount of the crystalline side phase for the $CaMoO_4$ was identified. It seems that this impurity phase effect reduces the amount of the $La_{2-x}Ca_xMo_2O_{9-x/2}$ homogeneous phase in the mixture and creates conditions for the formation of pure $La_2Mo_2O_9$ compound. This explains the increase in the phase transition enthalpy in $La_{1.9}Ca_{0.1}Mo_2O_{8.95}$ and $La_{1.85}Ca_{0.15}Mo_2O_{8.925}$ samples during both cooling stages (Figure 4). Meanwhile, by the further increase in the calcium substitution degree in the $La_{2-x}Ca_xMo_2O_{9-x/2}$ system, the decrease in the phase transition enthalpy is already determined by a significant lack of the $La_2Mo_2O_9$ crystalline phase. This conclusion is confirmed by the constant increase in the concentration of the crystalline phase of calcium molybdate in the final mixture of the obtained ceramics.

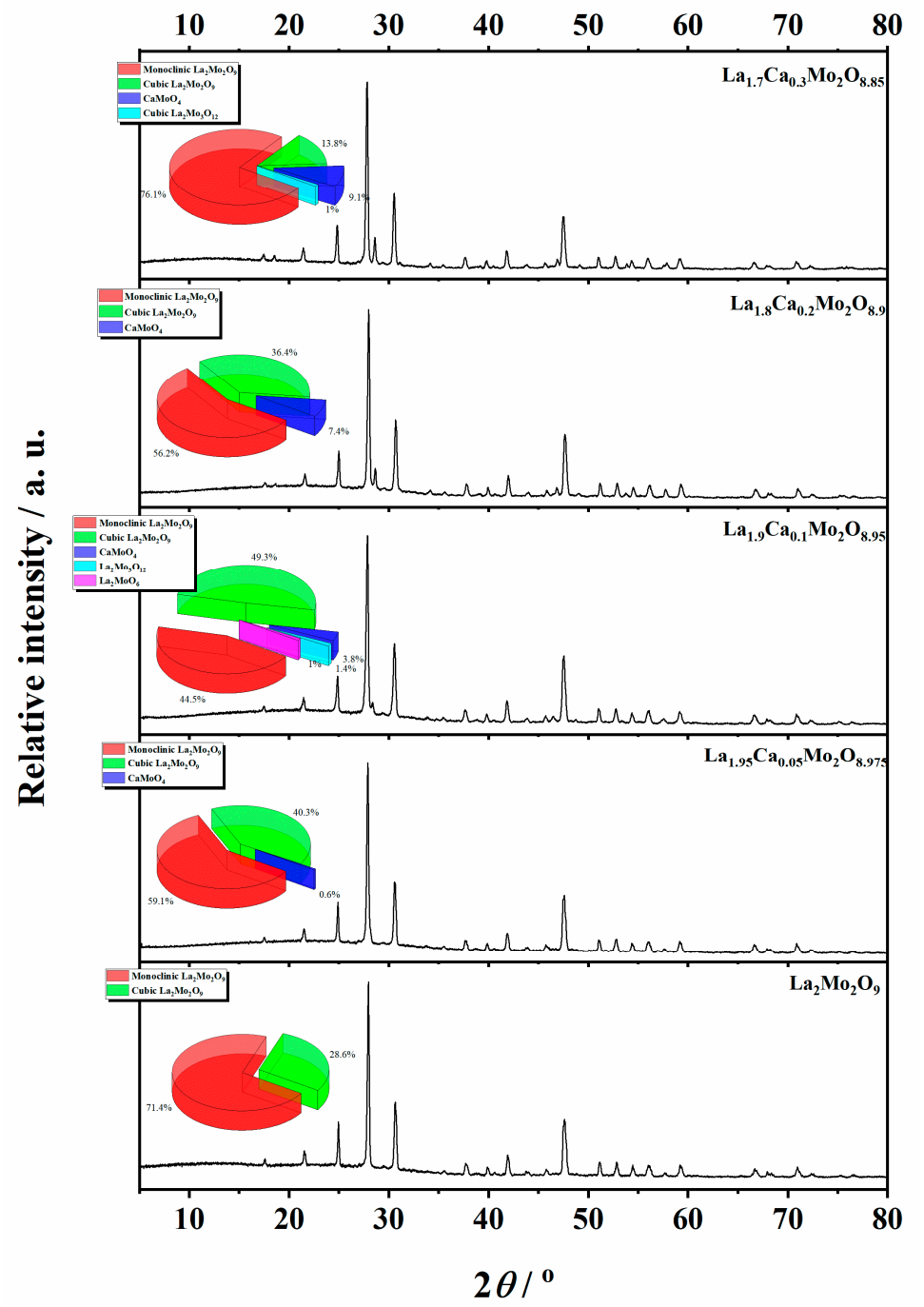

Figure 5. XRD patterns of the $La_{1-x}Ca_xMo_2O_{9-x/2}$ ceramic heat-treated at a 1000 °C temperature.

4. Conclusions

This study showed that the homogeneous substitution of lanthanum by calcium ions takes place up to the compound of initial composition for $La_{1.95}Ca_{0.05}Mo_2O_{8.975}$. In this case, the decrease in the phase transition enthalpy is determined by the increase in the concentration of the formation of the mixed compound for the initial composition of $La_{2-x}Ca_xMo_2O_{9-x/2}$. Meanwhile, the influence of the monoclinic phase amount on the phase transition enthalpy remained important only in the case of the formation of a pure $La_2Mo_2O_9$ compound, the amount of which significantly increases with the appearance of the $CaMoO_4$ impurity phase in the ceramic mixture. In summary, it can be concluded that the formation of the impurity of the calcium molybdate crystal phase, which compensates for the lack of lanthanum and the excess of molybdenum in the multicomponent oxide

$La_{2-x}Ca_xMo_2O_{9-x/2}$ system, has a significant influence on the decrease in the phase transition enthalpy in the $La_2Mo_2O_9$ compound. The influence of the monoclinic phase amount on the phase transition enthalpy remains an important factor only in the case of the pure lanthanum molybdate.

Author Contributions: A.Ž.: Conceptualization, Methodology, Software, Validation, Resources, Data curation, Writing—original draft, Writing—review and editing, Visualization, Supervision. G.G.: Methodology, Investigation, Resources. All authors have read and agreed to the published version of the manuscript.

Funding: This research received no external funding.

Institutional Review Board Statement: Not applicable.

Informed Consent Statement: Not applicable.

Data Availability Statement: The data presented in this study are available on request from the corresponding author.

Conflicts of Interest: The authors declare that they have no known competing financial interests or personal relationships that could have appeared to influence the work reported in this paper.

Appendix A

The DSC curves for the $La_{2-x}Ca_xMo_2O_{9-x/2}$ ceramic contain details and data supporting the results presented in Table 1. For comparison, the phase transition DSC curve for the $La_2Mo_2O_9$ compound is also presented in this section.

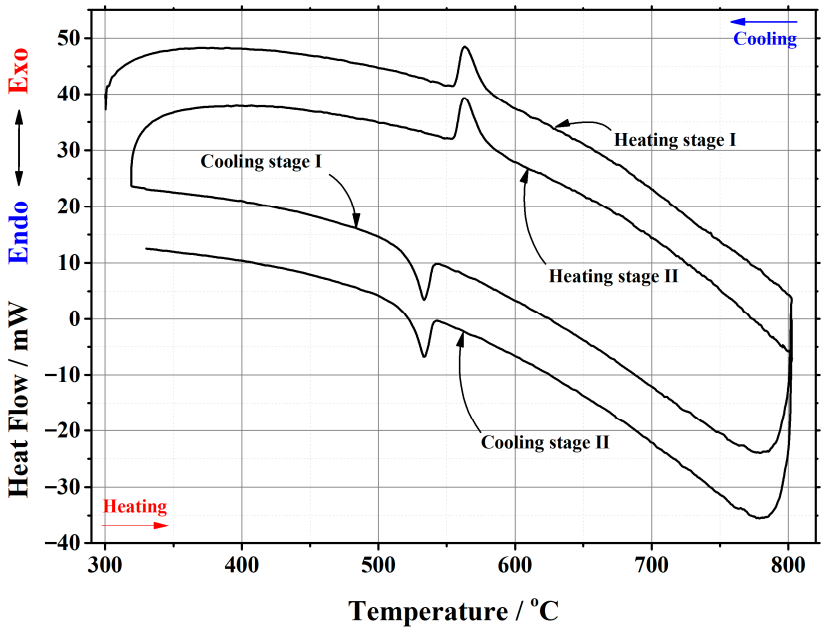

Figure A1. DSC curve of the phase transition cycles for $La_2Mo_2O_9$ ceramic heat-treated at 1000 °C.

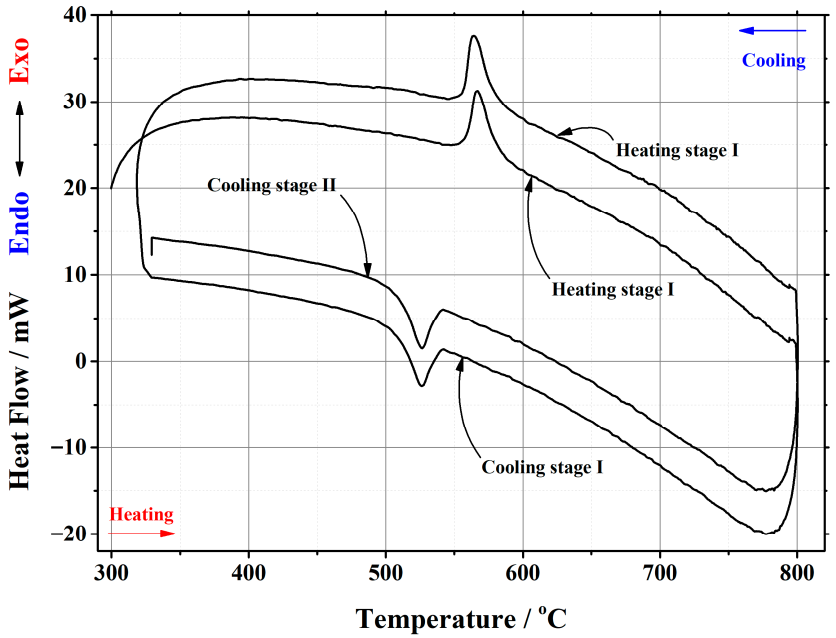

Figure A2. DSC curve of the phase transition cycles for $La_{1.999}Ca_{0.001}Mo_2O_{8.9995}$ ceramic heat-treated at 1000 °C.

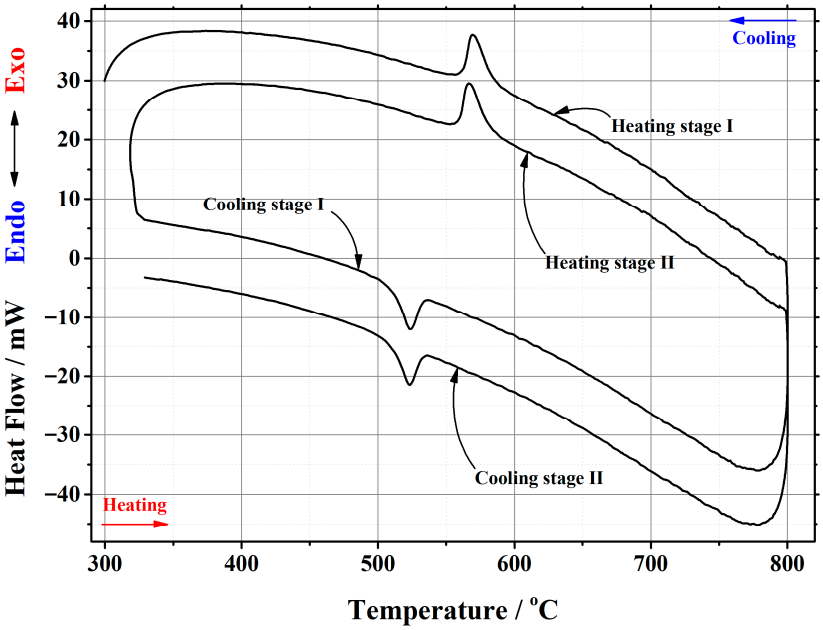

Figure A3. DSC curve of the phase transition cycles for $La_{1.99}Ca_{0.01}Mo_2O_{8.995}$ ceramic heat-treated at 1000 °C.

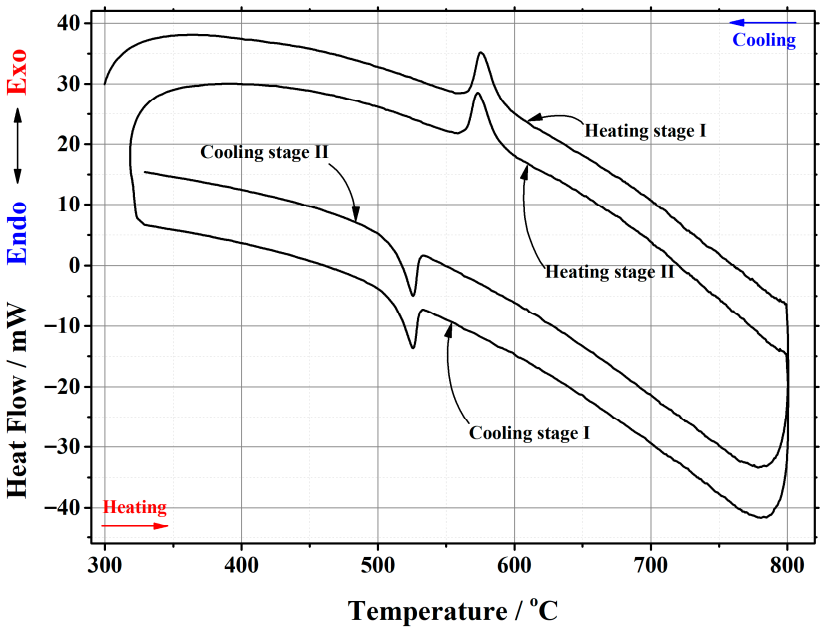

Figure A4. DSC curve of the phase transition cycles for $La_{1.9}Ca_{0.1}Mo_2O_{8.95}$ ceramic heat-treated at 1000 °C.

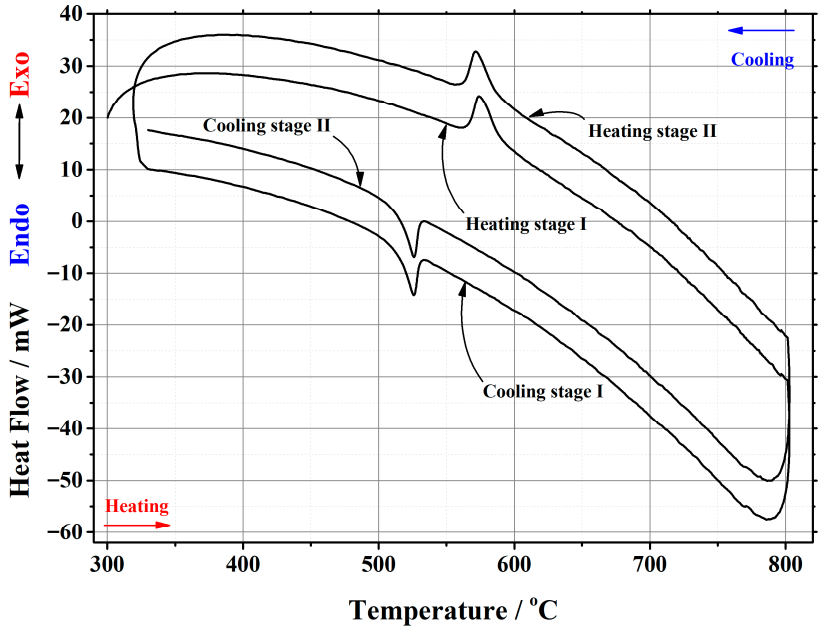

Figure A5. DSC curve of the phase transition cycles for $La_{1.85}Ca_{0.15}Mo_2O_{8.925}$ ceramic heat-treated at 1000 °C.

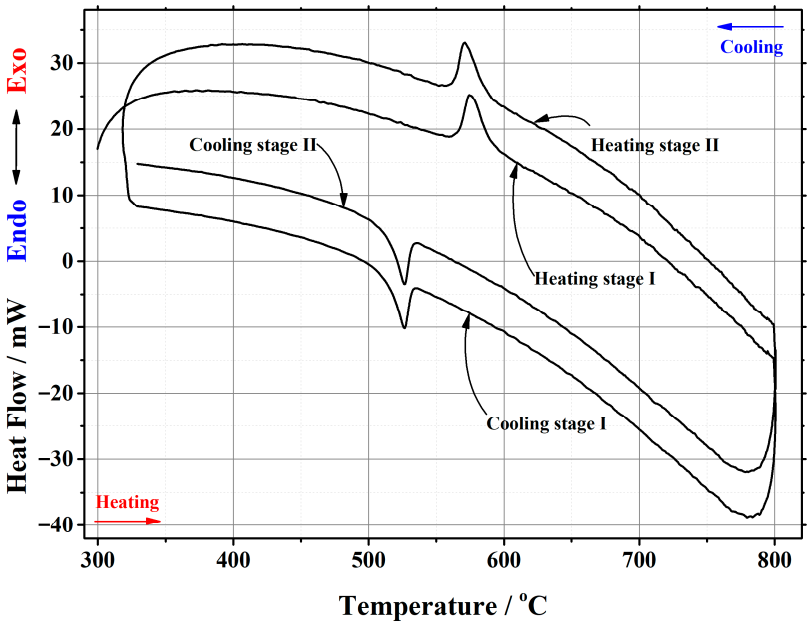

Figure A6. DSC curve of the phase transition cycles for $La_{1.8}Ca_{0.2}Mo_2O_{8.9}$ ceramic heat-treated at 1000 °C.

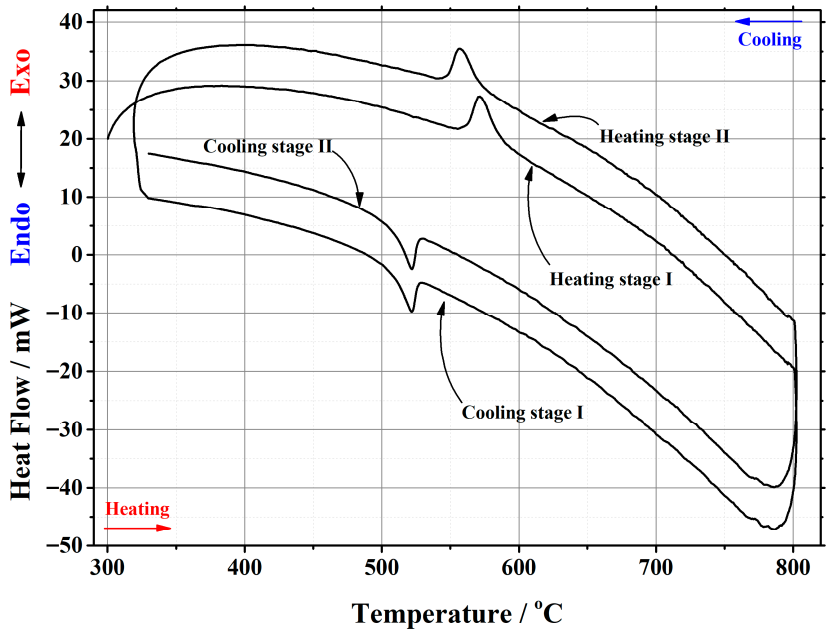

Figure A7. DSC curve of the phase transition cycles for $La_{1.75}Ca_{0.25}Mo_2O_{8.875}$ ceramic heat-treated at 1000 °C.

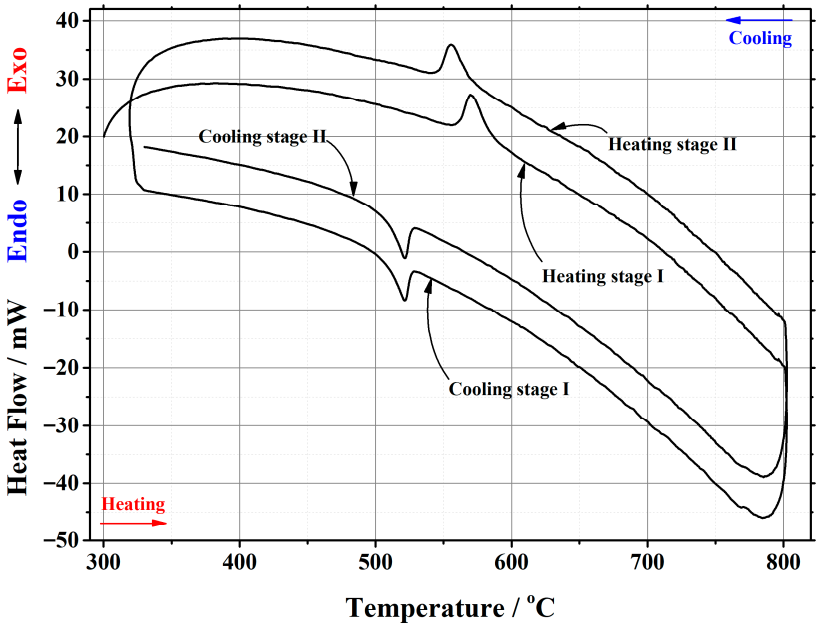

Figure A8. DSC curve of the phase transition cycles for $La_{1.7}Ca_{0.3}Mo_2O_{8.85}$ ceramic heat-treated at 1000 °C.

Appendix B

Rietveld refinement analysis results of the corresponding XRD patterns for the $La_{2-x}Ca_xMo_2O_{9-x/2}$ ceramic supporting the data presented in Table 2.

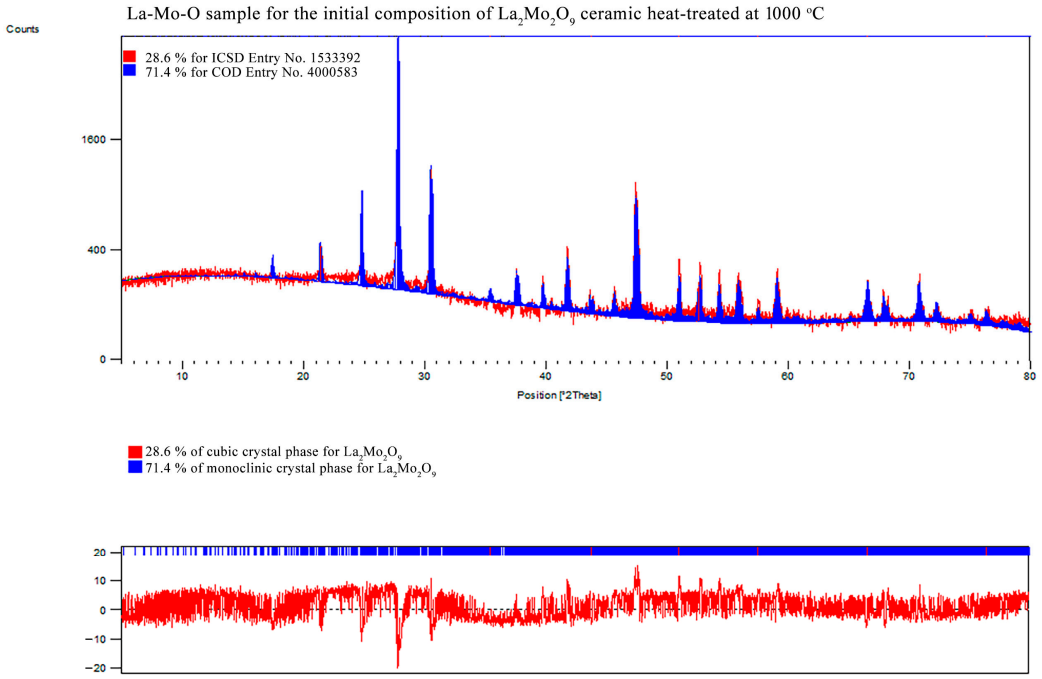

Figure A9. XRD pattern of the $La_2Mo_2O_9$ ceramic heat-treated at 1000 °C.

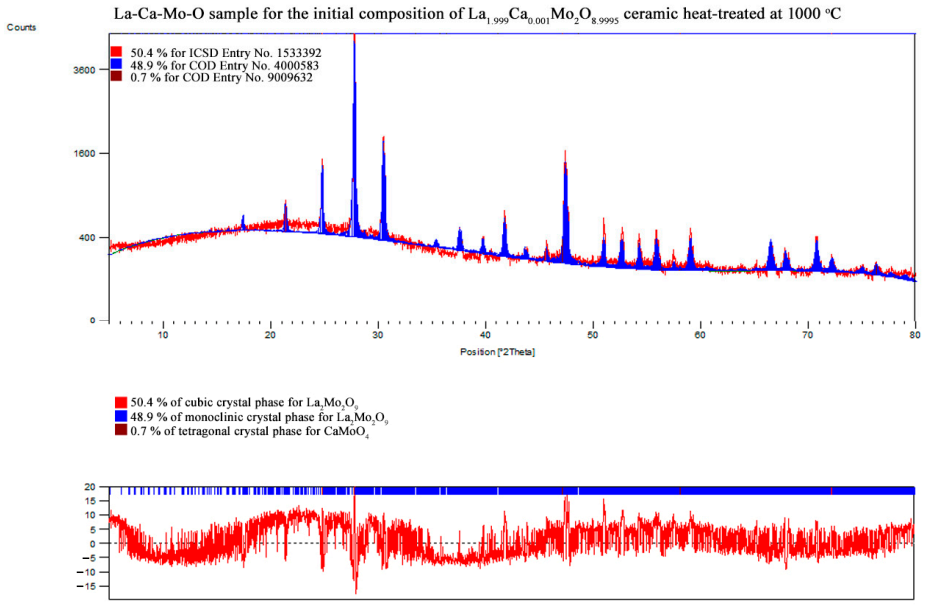

Figure A10. XRD pattern of the $La_{1.999}Ca_{0.001}Mo_2O_{8.9995}$ ceramic heat-treated at 1000 °C.

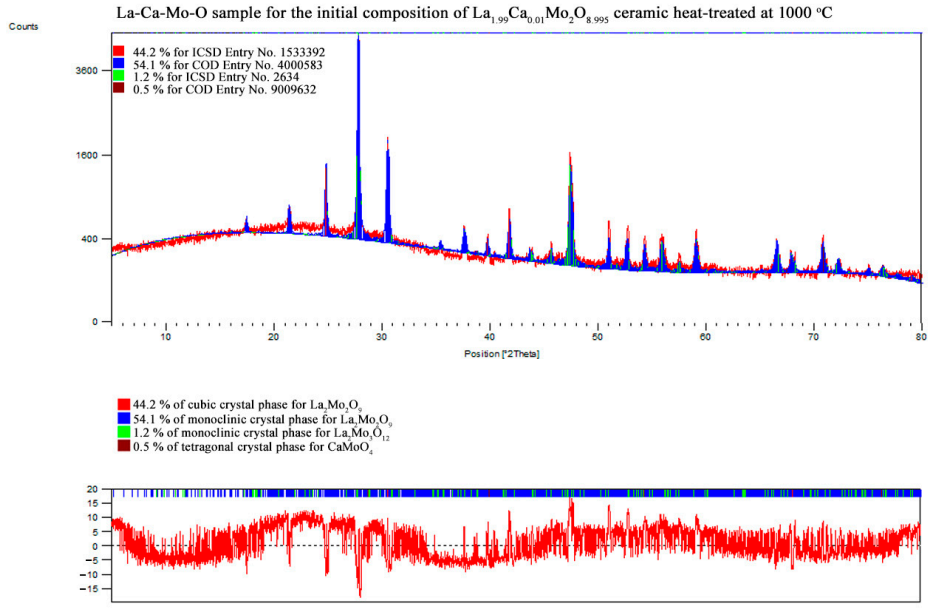

Figure A11. XRD pattern of the $La_{1.99}Ca_{0.01}Mo_2O_{8.995}$ ceramic heat-treated at 1000 °C.

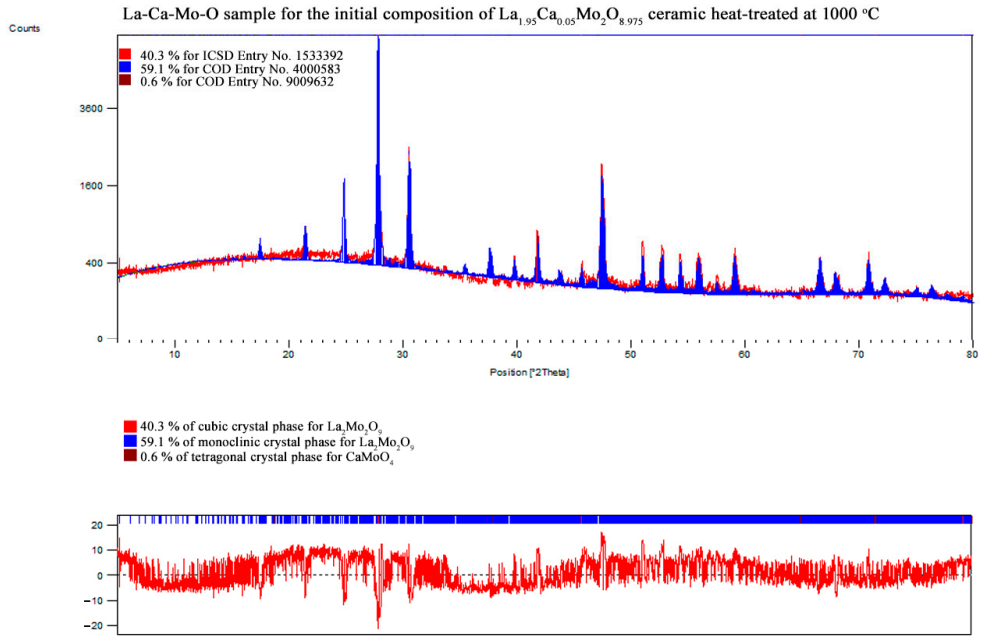

Figure A12. XRD pattern of the $La_{1.95}Ca_{0.05}Mo_2O_{8.975}$ ceramic heat-treated at 1000 °C.

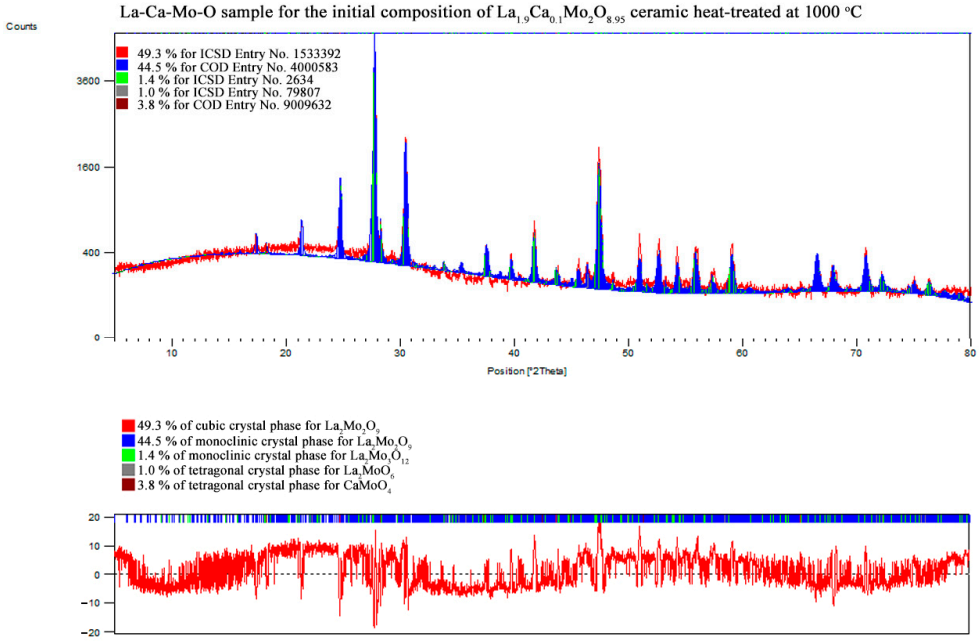

Figure A13. XRD pattern of the $La_{1.9}Ca_{0.1}Mo_2O_{8.95}$ ceramic heat-treated at 1000 °C.

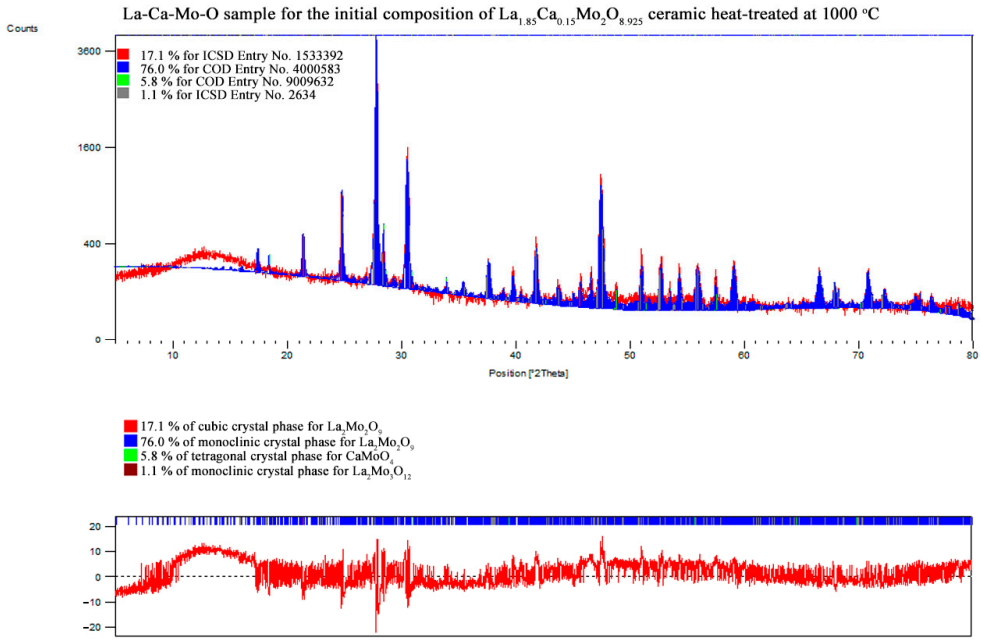

Figure A14. XRD pattern of the $La_{1.85}Ca_{0.15}Mo_2O_{8.925}$ ceramic heat-treated at 1000 °C.

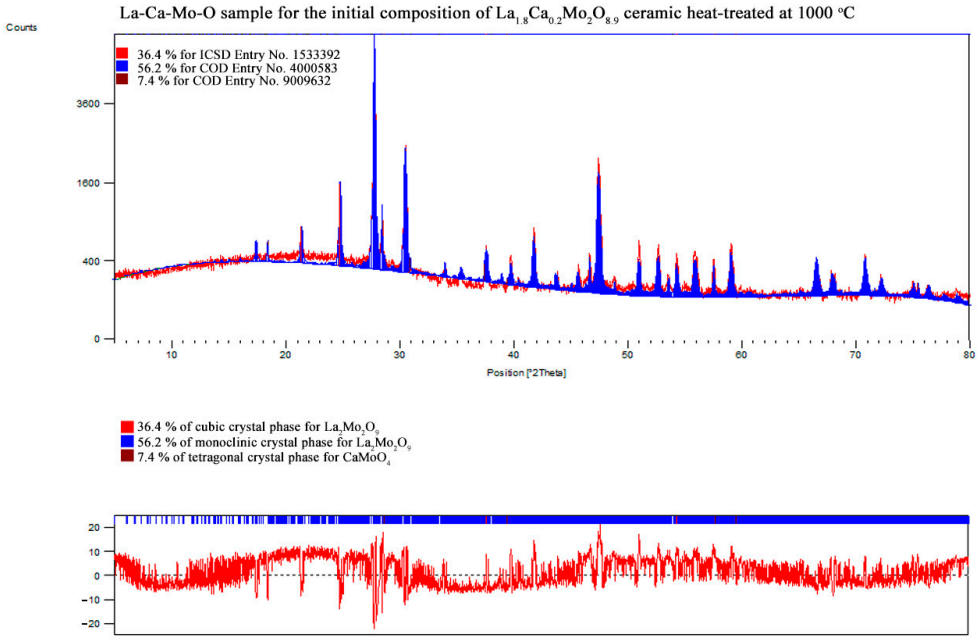

Figure A15. XRD pattern of the $La_{1.8}Ca_{0.2}Mo_2O_8$ ceramic heat-treated at 1000 °C.

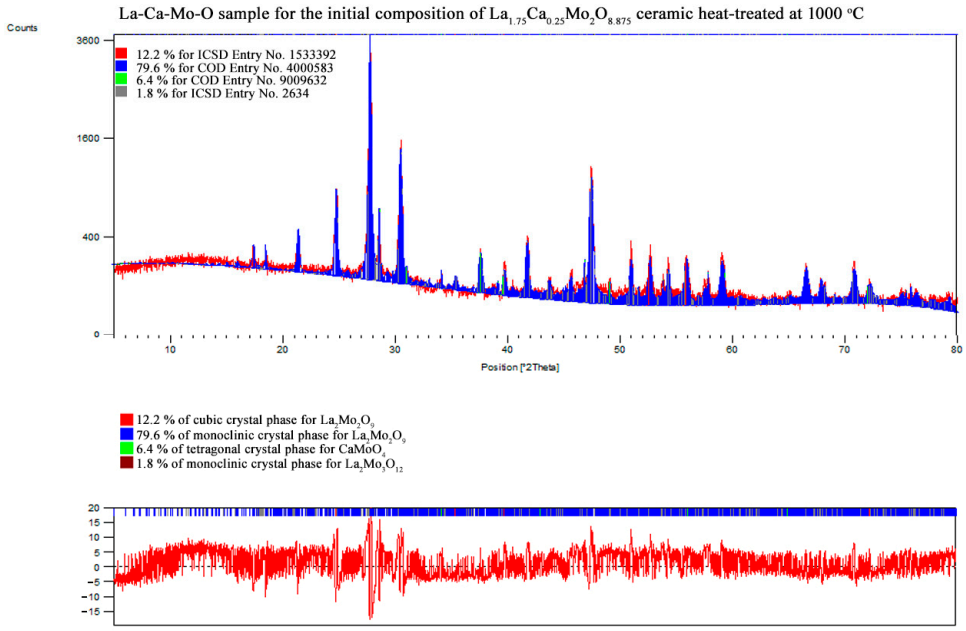

Figure A16. XRD pattern of the $La_{1.75}Ca_{0.25}Mo_2O_{8.875}$ ceramic heat-treated at 1000 °C.

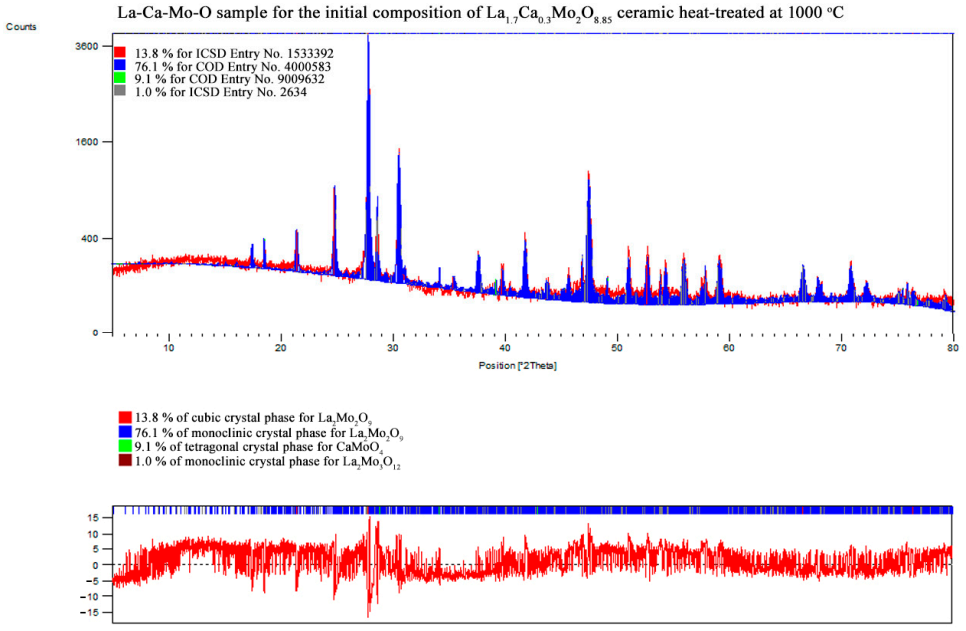

Figure A17. XRD pattern of the $La_{1.7}Ca_{0.3}Mo_2O_{8.85}$ ceramic heat-treated at 1000 °C.

References

1. Lacorre, P.; Goutenoire, F.; Bohnke, O.; Retoux, R.; Laligant, Y. Designing fast oxide-ion conductors based on $La_2Mo_2O_9$. *Nature* **2000**, *404*, 856–858. [CrossRef] [PubMed]
2. Skinner, S.J.; Kilner, J.A. Oxygen ion conductors. *Mater. Today* **2003**, *6*, 30–37. [CrossRef]
3. Yang, J.; Wang, Y.; Yang, B.; Tian, C.; Liu, Y.; Yang, L. Research progress of $La_2Mo_2O_9$-based oxide-ion conductor electrolyte materials. *Nanomater. Nanotechnol.* **2022**, *11*, 1–7. [CrossRef]
4. Jacquens, J.; Farrusseng, D.; Georges, S.; Viricelle, J.P.; Gaudillere, C.; Corbel, G.; Lacorre, P. Tests for the Use of $La_2Mo_2O_9$-based Oxides as Multipurpose SOFC Core Materials. *Fuel Cells* **2010**, *10*, 433–439. [CrossRef]
5. Lo, J.C.; Tsai, D.S.; Chen, Y.C.; Le, M.V.; Chung, W.H.; Liu, F.J. $La_2Mo_2O_9$-Based Electrolyte: Ion Conductivity and Anode-Supported Cell under Single Chamber Conditions. *J. Am. Ceram. Soc.* **2011**, *94*, 806–811. [CrossRef]
6. Kilner, J.; Druce, J.; Ishihara, T. Electrolytes. In *High-Temperature Solid Oxide Fuel Cells for the 21st Century: Fundamentals, Design and Applications: Second Edition*, 2nd ed.; Kendall, K., Kendall, M., Eds.; Elsevier Inc.: Amsterdam, The Netherlands, 2016; pp. 85–132. [CrossRef]

7. Siddharth Sil, A.; Bysakh, S. Effect of K doping on Mo^{6+} stability and ionic conductivity study in $La_2Mo_2O_9$ as oxide-ion conductor. *Mater. Res. Express* **2019**, *6*, 056203. [CrossRef]
8. Ali, M.; Wani, B.N.; Bharadwaj, S.R. Phase transition in LAMOX type compounds. *J. Therm. Anal. Calorim.* **2009**, *96*, 463–468. [CrossRef]
9. Zhang, H.; Wang, Y.; Wang, H.O.; Huo, D.X.; Tan, W.S. Room-temperature magnetoresistive and magnetocaloric effect in $La_{1-x}Ba_xMnO_3$ compounds: Role of Griffiths phase with ferromagnetic metal cluster above Curie temperature. *J. Appl. Phys.* **2022**, *131*, 043901. [CrossRef]
10. Evans, I.R.; Howard, J.A.K.; Evans, J.S.O. The crystal structure of alpha-$La_2Mo_2O_9$ and the structural origin of the oxide ion migration pathway. *Chem. Mater.* **2005**, *17*, 4074–4077. [CrossRef]
11. Goutenoire, F.; Isnard, O.; Retoux, R.; Lacorre, P. Crystal structure of $La_2Mo_2O_9$, a new fast oxide-ion conductor. *Chem. Mater.* **2000**, *12*, 2575–2580. [CrossRef]
12. Selmi, A.; Galven, C.; Corbel, G.; Lacorre, P. Thermal stability of alkali and alkaline-earth substituted LAMOX oxide-ion conductors. *Dalton Trans.* **2010**, *39*, 93–102. [CrossRef] [PubMed]
13. Tealdi, C.; Chiodelli, G.; Flor, G.; Leonardi, S. Electrode stability and electrochemical performance of Lamox electrolytes under fuel cell conditions. *Solid State Ionics* **2010**, *181*, 1456–1461. [CrossRef]
14. El Khal, H.; Cordier, A.; Batis, N.; Siebert, E.; Georges, S.; Steil, M.C. Effect of porosity on the electrical conductivity of LAMOX materials. *Solid State Ionics* **2017**, *304*, 75–84. [CrossRef]
15. Malavasi, L.; Fisher, C.A.J.; Islam, M.S. Oxide-ion and proton conducting electrolyte materials for clean energy applications: Structural and mechanistic features. *Chem. Soc. Rev.* **2010**, *39*, 4370–4387. [CrossRef] [PubMed]
16. Zhang, D.M.; Zhuang, Z.; Gao, Y.X.; Wang, X.P.; Fang, Q.F. Electrical properties and microstructure of nanocrystalline $La_{2-x}A_xMo_2O_{9-delta}$ (A = Ca, Sr, Ba, K) films. *Solid State Ionics* **2010**, *181*, 1510–1515. [CrossRef]
17. Corbel, G.; Durand, P.; Lacorre, P. Comprehensive survey of Nd^{3+} substitution In $La_2Mo_2O_9$ oxide-ion conductor. *J. Solid State Chem.* **2009**, *182*, 1009–1016. [CrossRef]
18. Khaled, A.; Pireaux, J.J.; Khelili, S. Synthesis and Characterization of Ca and Ba Doped LAMOX Materials and Surface Study by X-ray Photoelectron Spectroscopy. *Acta Chim. Slov.* **2012**, *59*, 766–778.
19. Das, A.; Lakhanlal, L.; Shajahan, I.; Dasari, H.P.; Saidutta, M.B.; Dasari, H. Dilatometer studies on LAMOX based electrolyte materials for solid oxide fuel cells. *Mater. Chem. Phys.* **2021**, *258*, 123958. [CrossRef]
20. Corbel, G.; Laligant, Y.; Goutenoire, F.; Suard, E.; Lacorre, P. Effects of partial substitution of Mo^{6+} by Cr^{6+} and W^{6+} on the crystal structure of the fast oxide-ion conductor structural effects of W^{6+}. *Chem. Mater.* **2005**, *17*, 4678–4684. [CrossRef]
21. Georges, S.; Bohnke, O.; Goutenoire, F.; Laligant, Y.; Fouletier, J.; Lacorre, P. Effects of tungsten substitution on the transport properties and mechanism of fast oxide-ion conduction in $La_2Mo_2O_9$. *Solid State Ionics* **2006**, *177*, 1715–1720. [CrossRef]
22. Pinet, P.; Fouletier, J.; Georges, S. Conductivity of reduced $La_2Mo_2O_9$ based oxides: The effect of tungsten substitution. *Mater. Res. Bull.* **2007**, *42*, 935–942. [CrossRef]
23. Kazakevicius, E.; Kezionis, A.; Kazlauskas, S.; Zalga, A.; Barre, M.; Juskenas, R. Phase transformations in $La_{2-x}Y_xMo_2O_9$ (x=0.05, x=0.075): Temperature cycling and DRT analysis. *Solid State Ionics* **2019**, *339*, 114989. [CrossRef]
24. Liao, Y.W.; Kawabata, S.; Yabutsuka, T.; Chen, W.J.; Okumura, H.; Takai, S. Low temperature phase transition phenomena in Ba- and Pb-substituted $La_2Mo_2O_9$ oxide ion conductors. *Solid State Ionics* **2020**, *354*, 115405. [CrossRef]
25. Acharya, S.; Naz, R. Nd-Nb co-dopant effect on suppression of phase transition, ionic conductivity and dielectrics relaxation phenomenon of $La_2Mo_2O_9$ system. *Ferroelectrics* **2022**, *589*, 243–251. [CrossRef]
26. Borah, L.N.; Sanjay; Pandey, A. Effect of Sn-doping at Mo-site on the conductivity of $La_2Mo_2O_9$ series of compounds. *Indian J. Phys.* **2010**, *84*, 699–704. [CrossRef]
27. Pahari, B.; Mhadhbi, N.; Corbel, G.; Lacorre, P.; Dittmer, J. Analysis of the local structure of phosphorus-substituted LAMOX oxide ion conductors. *Dalton Trans.* **2012**, *41*, 5696–5703. [CrossRef]
28. Dammak, K.; Mhadhbi, N.; Tozri, A.; Naili, H. Influence of Isovalent Partial Sulfur Substitution on the Structural, Thermal, Electrical and Spectroscopic Properties of $La_2Mo_2O_9$ Oxide Ion Conductors. *Eur. J. Inorg. Chem.* **2022**, e202200165. [CrossRef]
29. Paul, T.; Tsur, Y. Influence of Isovalent 'W' Substitutions on the Structure and Electrical Properties of $La_2Mo_2O_9$ Electrolyte for Intermediate-Temperature Solid Oxide Fuel Cells. *Ceramics* **2021**, *4*, 502–515. [CrossRef]
30. Selmi, A.; Corbel, G.; Kojikian, S.; Voronkova, V.; Kharitonova, E.; Lacorre, P. Complex effect of partial substitution of La^{3+} by Ca^{2+} on the stability of fast oxide-ion conductor $La_2Mo_2O_9$. *Eur. J. Inorg. Chem.* **2008**, 1813–1821. [CrossRef]
31. Porotnikova, N.; Khrustov, A.; Farlenkov, A.; Khodimchuk, A.; Partin, G.; Animitsa, I.; Kochetova, N.; Pavlov, D.; Ananyev, M. Promising $La_2Mo_2O_9$-$La_2Mo_3O_{12}$ Composite Oxygen-Ionic Electrolytes: Interphase Phenomena. *ACS Appl. Mater. Interfaces* **2022**, *14*, 6180–6193. [CrossRef]
32. Borah, L.N.; Pandey, A. Impedance Studies of $La_2Mo_{2-x}SnxO_{9-delta}$ Oxide Ion Conductors. *Acta Metall. Sin. (Engl. Lett.)* **2013**, *26*, 425–434. [CrossRef]
33. Le, M.V.; Tsai, D.S.; Yao, C.C.; Lo, J.C.; Vo, T.P.G. Properties of 10% Dy-doped $La_2Mo_2O_9$ and its electrolyte performance in single chamber solid oxide fuel cell. *J. Alloys. Compd.* **2014**, *582*, 780–785. [CrossRef]

34. Stankevičiūtė, R.; Žalga, A. Sol-gel synthesis, crystal structure, surface morphology, and optical properties of Eu_2O_3-doped $La_2Mo_3O_{12}$ ceramic. *J. Therm. Anal. Calorim.* **2014**, *118*, 925–935. [CrossRef]
35. Žalga, A.; Gaidamavičienė, G.; Gricius, Ž.; Užpurvytė, E.; Gadeikis, J.; Diktanaitė, A.; Barré, M.; Šalkus, T.; Kežionis, A.; Kazakevičius, E. Aqueous sol–gel synthesis, thermoanalytical study and electrical properties of $La_2Mo_2O_9$. *J. Therm. Anal. Calorim.* **2018**, *132*, 1499–1511. [CrossRef]